BOLETÍN DE LA SOCIEDAD ESPAÑOLA DE CERÁMICA Y VIDRIO XXX (2020) XXX–XXX

BOLETIN DE LA SOCIEDAD ESPAÑOLA DE
Cerámica y Vidrio
www.elsevier.es/bsecv

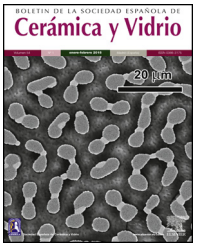

Original

Tuning $Ca_3Co_4O_9$ thermal and transport properties by TiC nanoparticles addition

Hippolyte Amaveda[a], *Oscar Juan Dura*[b], *Mario Mora*[a], *Miguel Angel Torres*[a], *Gabin Guelou*[c], *Maria Antonieta Madre*[a], *Sylvain Marinel*[c], *Andrés Sotelo*[a,*]

[a] *ICMA (Universidad de Zaragoza-CSIC), Dpto. de Ciencia y Tecnología de Materiales y Fluidos, C/ María de Luna 3, E-50018 Zaragoza, Spain*
[b] *Departamento de Física Aplicada (Universidad de Castilla-La Mancha), E-13071 Ciudad Real, Spain*
[c] *Normandie Univ, ENSICAEN, UNICAEN, CNRS, CRISMAT, 14000 Caen, France*

ARTICLE INFO

Article history:
Received 10 December 2019
Accepted 6 March 2020
Available online xxx

Keywords:
Ceramics
Oxides
Mechanical properties
ZT
Thermal expansion

ABSTRACT

$Ca_3Co_4O_9$ + x wt.% TiC (x = 0, 0.25, 0.5, 0.75, and 1.0) polycrystalline thermoelectric ceramics have been prepared through the classical ceramic route. XRD characterization has demonstrated that all samples are mainly composed by the $Ca_3Co_4O_9$ phase, while microstructural observation has shown that no reaction between both components has been produced. Moreover, TiC particles are well distributed for small additions, and start to agglomerate from 0.75 wt.% content. Density measurements showed that nearly no changes have been produced by TiC addition and nearly the whole porosity appears as open one. Furthermore, electrical resistivity decreases up to 0.75 wt.% addition, increasing for higher content. On the other hand, Seebeck coefficient has been maintained unchanged in all samples. In spite of an irregular behaviour of thermal conductivity with temperature, it tends to decrease when the temperature is raised, displaying the lowest values for the 0.25 wt.% samples. These data led to an increase of about 40% in ZT values at 800 °C for samples with 0.25 wt.% addition, when compared with the pure ones. Finally, linear thermal expansion coefficient is decreased when TiC content is increased, which can be exploited to fit the thermal expansion coefficients of all the components used to build a power generation thermoelectric module.

Ajuste de propiedades térmicas y eléctricas del $Ca_3Co_4O_9$ por medio de adición de nanopartículas de TiC

Palabras clave:
Cerámicas
Óxidos

RESUMEN

Se han preparado cerámicas de composición $Ca_3Co_4O_9$ + x% en peso de TiC (x = 0, 0,25; 0,5; 0,75, y 1,0) utilizando el método clásico de estado sólido. La caracterización por XRD mostró que la fase termoeléctrica $Ca_3Co_4O_9$ aparecía como mayoritaria. Las observaciones

* *Corresponding author.*
E-mail address: asotelo@unizar.es (A. Sotelo).
https://doi.org/10.1016/j.bsecv.2020.03.006

Please cite this article in press as: H. Amaveda, et al., Tuning $Ca_3Co_4O_9$ thermal and transport properties by TiC nanoparticles addition, Bol. Soc. Esp. Cerám. Vidr. (2020), https://doi.org/10.1016/j.bsecv.2020.03.006

Propiedades mecánicas
ZT
Dilatación térmica

microestructurales determinaron que no se produce reacción entre esta fase y las partículas de TiC. Estas partículas aparecen bien distribuidas cuando hay pequeñas adiciones y comienzan a aglomerarse a partir del 0,75% en peso. Las medidas de densidad indicaron que este parámetro no se modifica con la adición de TiC y, además, que se produce una porosidad de tipo abierto. La presencia de TiC modifica la resistividad eléctrica de forma que disminuye hasta el 0,75% en peso de TiC, aumentando para contenidos mayores, sin afectar el coeficiente de Seebeck. La conductividad térmica muestra un comportamiento irregular, pero tiende a disminuir al aumentar la temperatura, alcanzando los menores valores en muestras con 0,25% en peso de TiC. Estos resultados llevaron a un aumento del 40% en los valores de ZT a 800 °C en muestras con 0,25% TiC en peso, comparados con los medidos en muestras sin TiC. Finalmente, el coeficiente de dilatación lineal disminuye al aumentar el contenido de TiC, lo que puede utilizarse para ajustar los coeficientes de dilatación de todos los componentes al construir un módulo termoeléctrico de generación de potencia.

Introduction

Thermoelectric (TE) materials are characterized by their ability to transform a temperature difference into useful electrical power, provided by the Seebeck effect. The efficiency of these materials when considered for this energy conversion can be described through the ZT (dimensionless figure of merit). Physically it can be described by the expression $ZT = T\ S^2/\rho\ \kappa$, where T is the absolute temperature, S the Seebeck coefficient, ρ the electrical resistivity, and κ the thermal conductivity [1]. Due to their characteristics, these materials can harvest heat in many applications [2], or from renewable sources [3], to produce electrical power from a temperature gradient. Consequently, they can be used to exploit waste heat produced in non-renewable energy transformation systems, increasing, in this way, their efficiency [4,5]. Usually, for integration in commercial thermoelectric generators, these TE materials should display ZT values ≥ 1.

Today, there are TE commercially available devices, which are typically built using intermetallic legs. These intermetallic materials are characterized by high ZT values at relatively low temperatures [6–11]. Consequently, they are not useful at high temperatures due to the decrease of their performances, together with their high reactivity in these conditions under air, which leads to degradation processes or releasing heavy metals [12]. High temperature applications become feasible through the discovery of high TE performances in $Na_2Co_2O_4$ [13], which has led to intense research on this kind of materials and, to the discovery of new ones, as $Ca_3Co_4O_9$ [14,15] or $CuCrO_2$ [16], as *p*-type, and TiO- [17,18] or MnO-based materials [19] as n-type.

These Co-based materials can be crystallographically described using a monoclinic structure, which is formed by alternate stacking of two different layers. They are a conducting CoO_2 layer with CdI_2-type structure, and a rock-salt-type separating layer, acting as charge reservoir. Both layers have the same lattice parameters, only differing in their b-axis length, which leads to a misfit along this direction [20,21]. This high crystallographic anisotropy is reflected in the anisotropic grain growth, forming plate-like grains with favourable electrical conductivity along the ab-planes. These characteristics explain the large number of studies, which have been performed in the last years to obtain bulk materials with good grain orientation [22–27] to drastically decrease electrical resistivity with very slight modifications in the Seebeck coefficient values. On the other hand, many other works have also been studying the mechanisms to decrease thermal conductivity through different processes, as SiC nanoparticles addition, which can help to enhance phonon scattering [28,29]. The use of SiC nanoparticles has been justified as it is a semiconducting thermoelectric material with low electrical resistivity, as reported in [30], and it is able to decrease electrical resistivity and thermal conductivity without drastic modifications of Seebeck coefficient [28].

In spite of the large number of works published in the last years, it is very difficult to find studies reporting the materials characteristics from the point of view of their possible integration in practical thermoelectric modules, mostly related with their thermal expansion. This parameter is of the main importance, as it can be observed in the schematic presentation of a thermoelectric module of Fig. 1a, where the different types of materials are shown. The module consists in alternate *n* and *p* type thermoelectric materials, which are electrically connected in series and thermally in parallel. The connections between thermoelements are conducting materials (typically metals) to form the electric circuit. Moreover, the upper and lower parts of the module are electrically insulating materials (typically ceramics), which provide the mechanical robustness. Finally, all these materials are welded together to form the thermoelectric module. When heating this module, the situation is modified, as it can be seen in Fig. 1b, where the effect of different thermal expansion coefficients of thermoelements, is shown. The material with larger α will be subjected to compressive stress inside the module, while the one with lower α, to tensile stress. Consequently, these different stresses will affect the welding between different materials, which can degrade electrical connections and drastically affect the module performances and limiting its useful life.

Consequently, this work will report the results obtained in $Ca_3Co_4O_9$ ceramic materials with different additions of TiC nanoparticles. TiC has been chosen due to the relatively low mechanical properties of SiC, and especially very low

Please cite this article in press as: H. Amaveda, et al., Tuning $Ca_3Co_4O_9$ thermal and transport properties by TiC nanoparticles addition, Bol. Soc. Esp. Cerám. Vidr. (2020), https://doi.org/10.1016/j.bsecv.2020.03.006

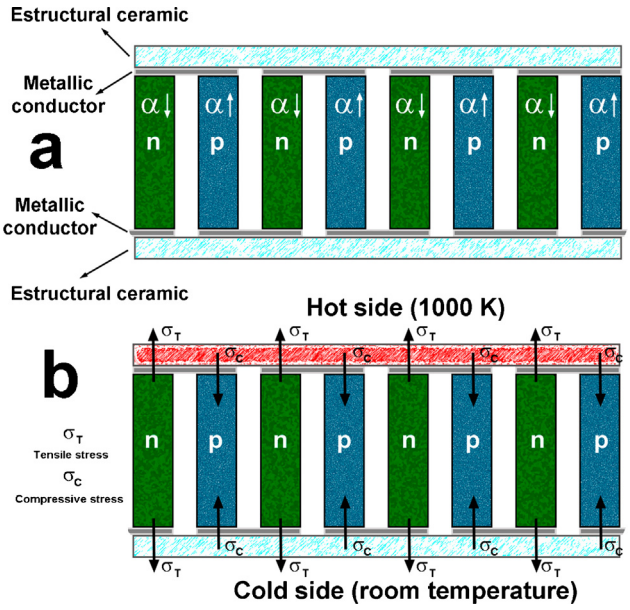

Fig. 1 – Schema showing the different types of materials present in a thermoelectric module (a); stresses appearing on the thermoelements when the module is operating (b). $\alpha\downarrow$ and $\alpha\uparrow$ are the low and high linear thermal expansion coefficients; σ_T, and σ_C are the tensile and compressive stresses.

fracture toughness [31]. Moreover, TiC addition to SiC has drastically increased mechanical properties in around 50% flexural strength, and two times for fracture toughness [32]. Furthermore, TiC is characterized by relatively good TE properties except by a very low Seebeck coefficient [33]. The effect of these additions on the structural, and microstructural properties will be studied and related to the thermal, and electrical properties of the final sintered materials.

Experimental

$Ca_3Co_4O_9$ + x wt.% TiC nanoparticles, with x = 0.00, 0.25, 0.50, 0.75, and 1.0, have been prepared using the classical solid state route. The amount of TiC added to the samples has been fixed taking into account the optimal content of SiC nanoparticles in $Bi_2Sr_2Co_2O_y$, which is much lower than 1 wt.% [28]. For this purpose, $CaCO_3$ (Panreac, 98 + %), and Co_2O_3 (Aldrich, 98 + %), were weighed in stoichiometric proportions, mixed and ball milled 30 min at 300 rpm in water media. The powder suspension was dried under infrared radiation, followed by manual milling, and two-step calcination procedure at 750 and 800 °C for 12 h under air, with an intermediate manual milling, to decompose the Ca carbonate and produce prereacted materials, as previously reported [34]. After manually milling these calcined powders, TiC (Aldrich, <200 nm) was added in the adequate proportions and ball milled again for 30 min at 300 rpm to obtain a homogeneous mixture. The different mixtures were then cold uniaxially pressed into pellets under 400 MPa, followed by sintering at 900 °C for 24 h under air atmosphere, and a final furnace cooling at room temperature.

Powder X-ray diffraction (XRD) patterns were obtained at room temperature in a theta-theta PANalyticalX'Pert Pro diffractometer (CuKα radiation, λ = 1.54059 Å) between 10° and 40°, where the main peaks of $Ca_3Co_4O_9$ phase appear. Moreover, Rietveld refinement has been used to determine lattice parameters. Density measurements were performed using both Archimedes' method and in a He pycnometer (AccuPyc 1340 from micromeritics) on several sintered samples for each composition. The relative density values were calculated with respect to the theoretical one of $Ca_3Co_4O_9$ (4.677 g/cm^3 [35]) and TiC (4.93 g/cm^3 [36]).

Microstructural observations have been performed on several longitudinal fractured sections of samples, using a Field Emission Scanning Electron Microscope (FESEM, Carl Zeiss Merlin) fitted with an energy-dispersive spectrometry (EDS) system. Several micrographs obtained in each specimen have been used to determine the phases formed in each sample. Mechanical properties were measured in four samples of each composition by the three points bending test, in an Instron 5565 testing machine with 10 mm span and a punch displacement of 30 μm/s. Electrical resistivity and Seebeck coefficient were simultaneously measured using the standard four point contact in a LSR-3 measurement device (Linseis GmbH) between 50 and 800 °C under He atmosphere. Thermal diffusivity (α) has been obtained using a laser-flash system (Linseis LFA 1000). The thermal conductivity (κ) has been determined using $\kappa = \alpha\ C_p\ \rho$, where C_p is the specific heat and ρ is the sample density previously determined. Specific heat was calculated using the well-known Dulong–Petit law. Using electrical resistivity, Seebeck coefficient, and thermal conductivity data, ZT evolution with temperature has been calculated to determine the samples performances. The samples characteristics have been compared with the results obtained in pure ones and with the best values reported in the literature. Finally, dilatometric characterization has been performed between room temperature and 800 °C in a L79 HCS dilatometer (Linseis GmbH) in order to evaluate the linear expansion coefficient variation as a function of the amount of TiC addition.

Results and discussion

Powder XRD patterns determined in all $Ca_3Co_4O_9$ + x wt.% TiC samples (with x = 0, 0.25, 0.5, 0.75, and 1) are displayed in Fig. 2. In the graph, it can be observed that all samples present the same patterns, independently of the TiC addition, and most of the peaks can be associated to the $Ca_3Co_4O_9$ phase (with monoclinic symmetry) diffraction planes [37,38]. Moreover, the highest peaks have been indexed as corresponding to the ab-planes, indicating some degree of texture in the powders, which is induced by the samples preparation [39]. On the other hand, only small amounts of $Ca_3Co_2O_6$ phase (indicated by * [40]), besides the thermoelectric one, have been identified with this technique, due to the small amount and sizes of TiC added to the samples. Furthermore, no shift has been detected in the peaks position, clearly showing that no cationic substitution has been produced in the $Ca_3Co_4O_9$ phase. This fact has been confirmed through the close view of one of the main peaks of $Ca_3Co_4O_9$ phase, (002) and presented in Fig. 3. As it can be easily observed in the plot, no significant shift of the

Please cite this article in press as: H. Amaveda, et al., Tuning $Ca_3Co_4O_9$ thermal and transport properties by TiC nanoparticles addition, Bol. Soc. Esp. Cerám. Vidr. (2020), https://doi.org/10.1016/j.bsecv.2020.03.006

Table 1 – Lattice parameters obtained after Rietveld refinement of XRD patterns of all samples.

TiC content (wt.%)	a (Å)	$b1$ (Å)	$b2$ (Å)	c (Å)	β (°)
0	4.8314	4.5492	2.8264	10.8477	98.11
0.25	4.8337	4.5612	2.8356	10.8458	98.19
0.5	4.8350	4.5606	2.8295	10.8476	98.23
0.75	4.8337	4.5622	2.8330	10.8476	98.17
1	4.8341	4.5581	2.8358	10.8596	98.55
Ref. [41]	4.8271	4.5615	2.8173	10.8300	98.14

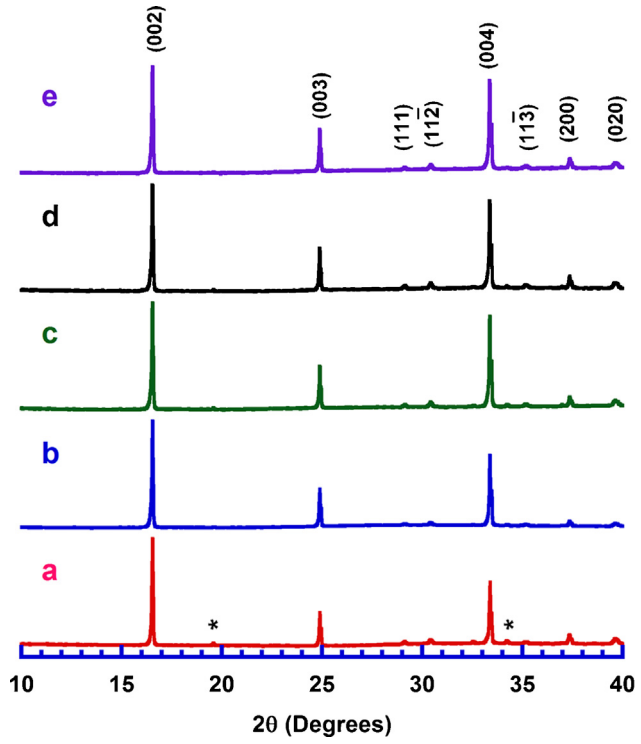

Fig. 2 – Powder X-ray diffraction patterns obtained for the $Ca_3Co_4O_9 + x$ wt.% TiC samples; $x = 0.00$ (a); 0.25 (b); 0.50 (c); 0.75 (d); and 1.0 (e). The diffraction planes index the reflections belonging to the $Ca_3Co_4O_9$ phase, and * the ones for the $Ca_3Co_2O_6$ one.

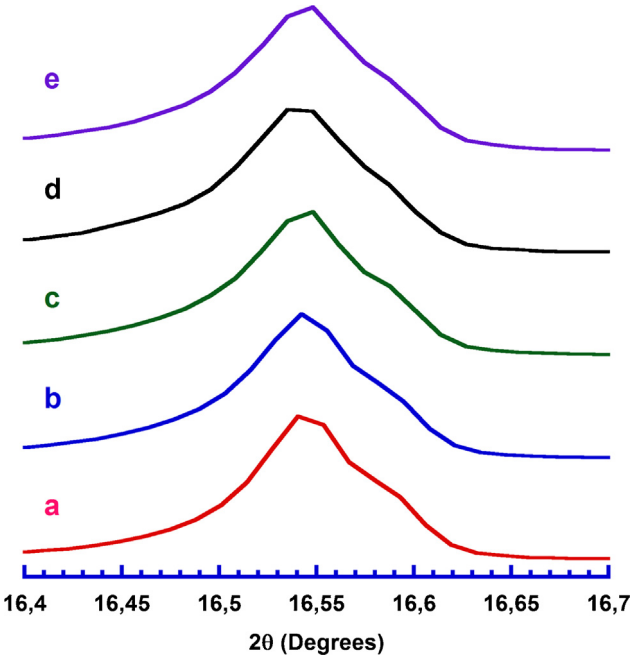

Fig. 3 – Enlarged view of the (002) diffraction peak in the $Ca_3Co_4O_9 + x$ wt.% TiC samples; $x = 0.00$ (a); 0.25 (b); 0.50 (c); 0.75 (d); and 1.0 (e).

peak has been produced, independently of the TiC addition, reflecting that Ti has not diffused into the crystal structure of the thermoelectric phase. Moreover, lattice parameters have been calculated from the Rietveld refinement of each pattern and they are presented in Table 1, together with the reported in literature [41]. As it can be observed in these data, there are differences between the parameters determined in these samples and the previously reported in the literature, but they could be associated to the typical texture-induced problems due to the plate-like nature of the thermoelectric grains. Consequently, it could be deduced that no significant element substitution has been produced.

In Fig. 4 some representative SEM micrographs, performed on the fractured surfaces of samples, are presented. In these images, it is easy to see that all samples are composed of randomly oriented plate-like grains, which is the typical microstructure obtained through the classical solid-state method. Moreover, the images show a slight increase of grain sizes when the amount of TiC nanoparticles is raised. In order to confirm this observation, grain sizes have been evaluated on several micrographs for each composition using the line intercept method. The mean grain sizes have been 5.24, 5.59, 5.74, 5.85, and 5.92 μm, for the 0, 0.25, 0.50, 0.75, and 1.0 wt.% TiC addition, respectively. However, porosity seems to be nearly unchanged in all samples, which can be easily explained taking into account the relatively low sintering temperature used in this work, which is limited by the maximum stability temperature of $Ca_3Co_4O_9$ phase (926 °C). This temperature is far from the necessary to form a liquid phase in this system (~1350 °C) [42], hindering the samples densification during sintering. Additionally, it is also very far from the melting point of TiC (3067 °C) [36], which cannot help in the sintering process. On the other hand, TiC has been found to be well distributed all around the samples for ≤ 0.5 wt%, while for higher contents, TiC starts to form agglomerates (indicated by an arrow in Fig. 4c) which are placed between the thermoelectric grains. A closer view of these agglomerates is shown in the insert in Fig. 4c, for clarity. On the other hand, EDS analysis of these agglomerates cannot give a clear indication of the possible oxidation of TiC during sintering process, even if it has been reported for the pure compound, or the TiC/SiC composite,

Please cite this article in press as: H. Amaveda, et al., Tuning $Ca_3Co_4O_9$ thermal and transport properties by TiC nanoparticles addition, Bol. Soc. Esp. Cerám. Vidr. (2020), https://doi.org/10.1016/j.bsecv.2020.03.006

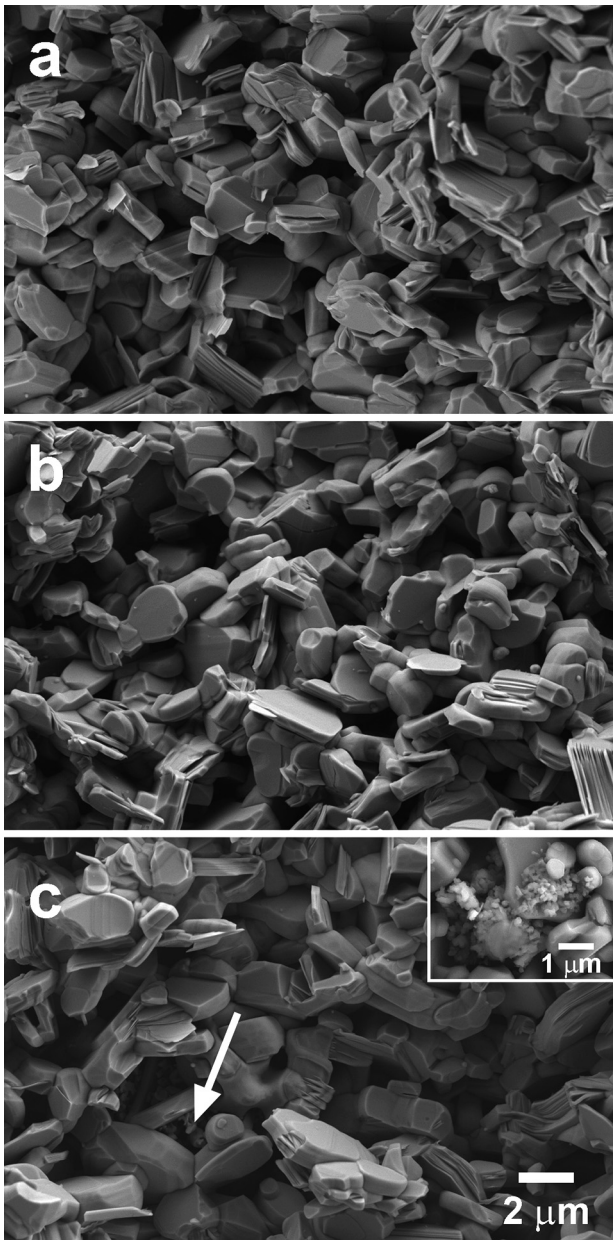

Fig. 4 – Representative SEM micrographs performed in fractured surfaces of $Ca_3Co_4O_9$ + x wt.% TiC samples, for x = 0.00 (a); 0.25 (b); and 0.75 (c). The arrow indicates a TiC agglomerate, with a closer view in the insert, for clarity.

in previous works [43,44]. However, TiC oxidation should not negatively affect transport properties, as TiO_2 doping has been shown to decrease electrical resistivity of $Ca_3Co_4O_9$ material [45].

In order to confirm the microstructural evolution observed in the SEM micrographs, which showed that no modification in the porosity content has been produced by TiC addition, the samples density, evaluated through Archimedes' method, has been determined on 4 samples for each composition. In order to minimize measurement errors, they were measured and weighed for three times, and the obtained results are summarized in Table 2. As it can be deduced from these data,

Table 2 – Relative density of sintered samples determined through Archimedes' method and He pycnometer; and mean thermal expansion coefficient.

TiC content (wt.%)	Relative density (%) Archimedes	α (10^{-6} K^{-1}) He picnometer	
0	73.0 ± 0.8	96.0 ± 1.0	10.34
0.25	74.2 ± 1.0	98.4 ± 1.0	9.94
0.5	75.0 ± 1.3	98.7 ± 1.0	9.92
0.75	74.9 ± 1.1	98.9 ± 1.0	9.90
1	74.1 ± 0.9	98.6 ± 1.0	9.57

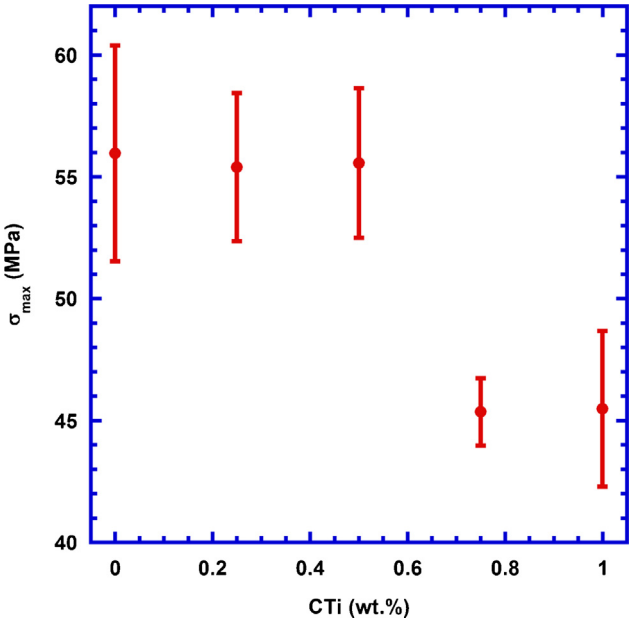

Fig. 5 – Three point bending stress values, together with their standard error, as a function of TiC content.

all samples display very similar values, being slightly higher when TiC is added, in agreement with the SEM observations. The data clearly point out that TiC has no influence on the densification of samples during sintering procedure. Moreover, these values are of the order or higher than the reported for classically sintered $Ca_3Co_4O_9$ materials [26,46–48]. On the other hand, density measurements have been also performed in an He pycnometer in order to distinguish between open and close porosity. The obtained data clearly showed that nearly the whole porosity found in the samples is open one, as the density values are nearly 100% of the theoretical one (see Table 2).

These results are reflected on the mechanical properties of these samples, determined through three points bending tests, and the results are displayed in Fig. 5, together with the corresponding measurement errors. As it can be deduced from the graph, the TiC addition in small amounts (≤0.5 wt.%) does not significantly modify mechanical properties, when compared with pure $Ca_3Co_4O_9$ samples, while higher content decreases them in a relatively important manner due to the agglomeration of TiC particles between the thermoelectric grains (see Fig. 4c). The fact that the mechanical properties are maintained for low TiC additions can be explained by the regular distribution of TiC grains between the thermoelectric

Please cite this article in press as: H. Amaveda, et al., Tuning $Ca_3Co_4O_9$ thermal and transport properties by TiC nanoparticles addition, Bol. Soc. Esp. Cerám. Vidr. (2020), https://doi.org/10.1016/j.bsecv.2020.03.006

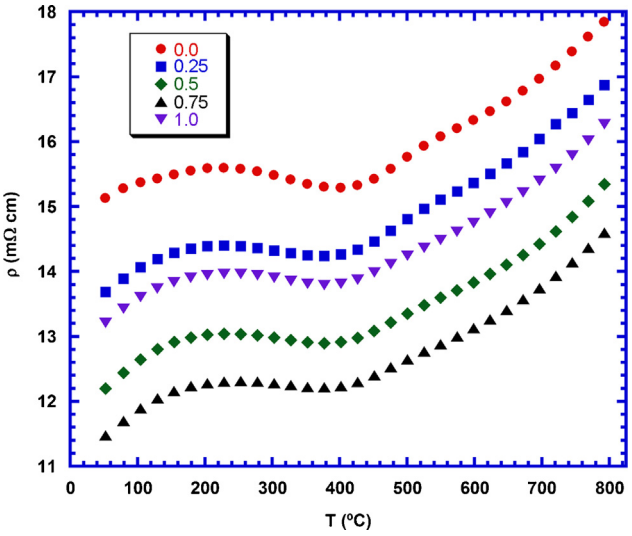

Fig. 6 – Electrical resistivity evolution with temperature and TiC content in $Ca_3Co_4O_9$ + x wt.% TiC samples.

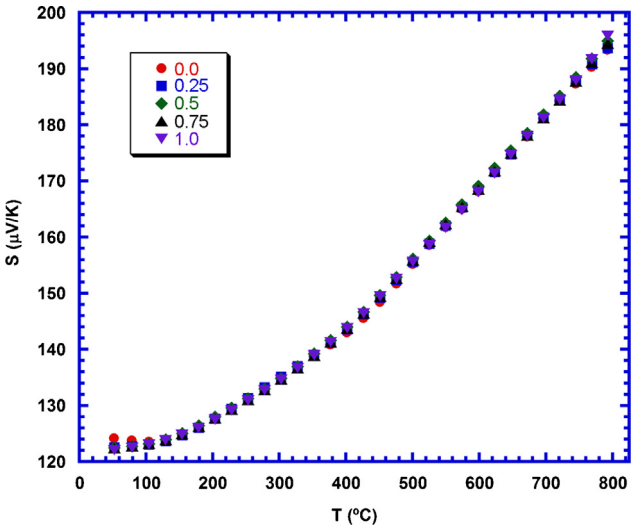

Fig. 7 – Seebeck coefficient evolution with temperature and TiC content in $Ca_3Co_4O_9$ + x wt.% TiC samples.

ones, as observed in the SEM micrographs, which is counteracted by the thermoelectric grains growth. In the case of high TiC content, the decrease is associated to the agglomeration of TiC particles already observed and mentioned in the SEM discussion, which leads to the formation of weak zones in the samples. On the other hand, the large amount of porosity in these sintered samples lead to much lower mechanical properties than the reported in nearly fully dense materials (287 MPa) [49].

The electrical resistivity evolution with temperature and the TiC content is shown in Fig. 6. As it can be observed in the graph, all samples display the same behaviour in the whole measured temperature range. On the other hand, TiC addition promotes a decrease of electrical resistivity, when compared with the samples without additions. It can be associated to the slight increase of grain sizes which leads to the opposite effect produced by TiC nanoparticles, which can scatter charge carriers. Moreover, the low electrical resistivity values of TiC material [33] can help to reduce electrical resistivity in the grain boundaries, as it has been reported for the addition of other conducting materials [50,51]. Moreover, electrical resistivity decreases when the TiC content is increased up to 0.75 wt.%, increasing for further addition. This increase for the highest TiC containing samples can be explained by the agglomeration of TiC nanoparticles, which can limit the charge carrier mobility due to the very large amount of grain boundaries in these regions. The lowest measured resistivity values at 800 °C (14.5 mΩ cm for the 0.75 wt.% TiC samples) are around the best values obtained for $Ca_3Co_4O_9$ samples sintered and textured by spark plasma sintering (15–18 mΩ cm) [52] and about 15% lower than the pure $Ca_3Co_4O_9$ samples prepared in this work. On the other hand, they are higher than the reported for fully dense materials prepared through alternative methods (10 mΩ cm) [53].

Fig. 7 shows the variation of S with temperature, as a function of the TiC nanoparticles addition. The graph clearly shows that S is positive at all temperatures, confirming a conduction mechanism mainly produced by holes. The values of the Seebeck coefficient increase with temperature, and display the same vales for all the samples. This behaviour can be explained when considering the very small contribution of TiC to the S values of these samples [33]. Consequently, the total S values, which have been measured in these samples are only due to the $Ca_3Co_4O_9$ contribution, and it is the same for all of them. The highest S value has been determined at 800 °C (around 195 μV/K) is higher than the best values reported for pure $Ca_3Co_4O_9$ samples sintered and textured by spark plasma sintering (170–175 μV/K) [52]. On the other hand, it is lower than the measured in highly dense materials prepared through alternative methods (205 μV/K) [53].

The temperature dependence of the thermal conductivity, as a function of TiC content, is plotted in Fig. 8. As it can be observed in the graph, in spite of the irregular variation with temperature, thermal conductivity shows a tendency to

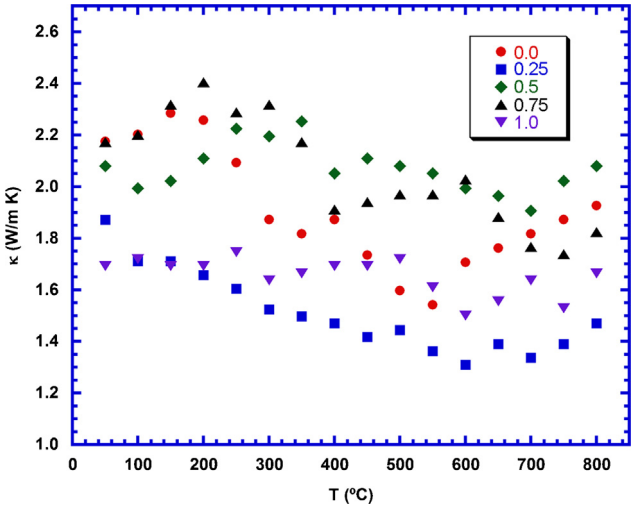

Fig. 8 – Thermal conductivity evolution with temperature and TiC content in $Ca_3Co_4O_9$ + x wt.% TiC samples.

Please cite this article in press as: H. Amaveda, et al., Tuning $Ca_3Co_4O_9$ thermal and transport properties by TiC nanoparticles addition, Bol. Soc. Esp. Cerám. Vidr. (2020), https://doi.org/10.1016/j.bsecv.2020.03.006

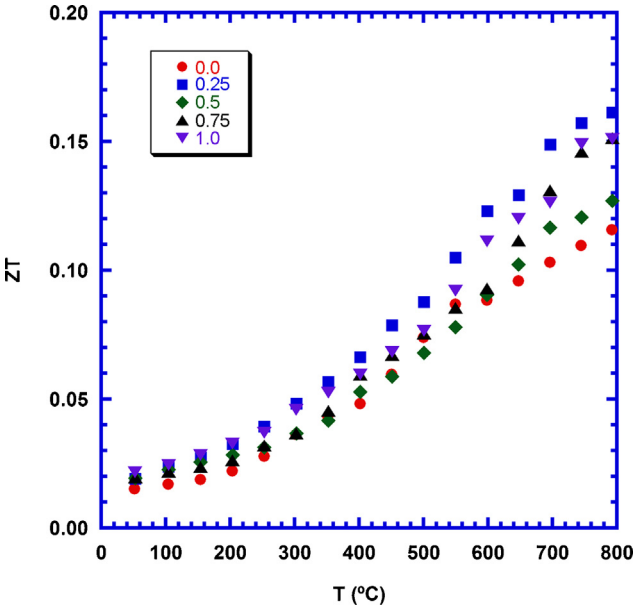

Fig. 9 – ZT evolution with temperature and TiC content in $Ca_3Co_4O_9$ + x wt.% TiC samples.

decrease when the temperature is raised. On the other hand, the samples do not show a regular evolution with the TiC content, and only the 0.25 wt.% TiC added sample displays a clear lower value than the other samples, in the whole measured temperature range. The low values obtained in these samples are consistent with their high amount of porosity. The minimum value measured in these samples at 800 °C (1.45 W/K m) is much lower than the reported in hot-pressed samples (2.2, 3, and 4.7 W/K m) [54–56], measured along the ab-plane, or sintered through Spark Plasma Sintering (SPS, 2.1 W/K m) [57]. On the other hand, it is higher than the measured in classically sintered materials (0.9 W/K m) [55] with much lower density (60% of the theoretical) than the samples presented in this work (>70%).

The samples performances have been calculated through ZT, and presented in Fig. 9 as a function of temperature and TiC content. As it can be observed in the plot, at 800 °C the highest increase is obtained for the 0.25 wt.%TiC (0.16), which is ~40% higher than the determined in pure ones. Moreover, it is in the order of the reported for textured samples (0.18, and 0.16 [54,55]), or sintered through SPS (0.15 [57]). On the other hand, it is lower than the measured in Sr-doped textured materials (0.29 [56]), but much higher than the reported for classically sintered materials (0.08 [55]). It is important to highlight that the results presented in this work have been obtained through a very simple and scalable method without the need of long processes or expensive equipment.

Finally, thermal expansion coefficient has been determined as a very important parameter when considering these materials for integration in power generation modules. The mean values determined in all samples, as a function of TiC content, are displayed in Table 2. As it can be deduced from these data, linear thermal expansion coefficient for the pure sample is 10.34 10^{-6} K^{-1}, and it is decreased when TiC is added. Moreover, it is further decreased when the TiC content is increased, reaching the minimum values (9.57 10^{-6} K^{-1}) for the highest TiC addition (about 10% decrease, when compared to the pure $Ca_3Co_4O_9$ one), and lower than the measured in pure and Bi-doped $Ca_3Co_4O_9$ (between 10.6 10^{-6} K^{-1} and 12.8 10^{-6} K^{-1}) [46]. Unfortunately, in the best of our knowledge there are not many data available for this compound, but they are in the order of the typically reported for the pure and doped $Bi_2AE_2Co_xO_y$ compounds (AE = Ca, Sr, and Ba, and x = 1.7, 1.8, and 2, respectively) [58].

All these data clearly point out that the addition of foreign compounds to the $Ca_3Co_4O_9$ are useful, not only to improve thermoelectric performances without drastically modifying mechanical ones, but also to tune the thermal expansion coefficient to make it fitting with the one of the different components used to build the thermoelectric modules.

Conclusions

This work has shown that $Ca_3Co_4O_9$ + x wt.% TiC (x = 0, 0.25, 0.5, 0.75, and 1.0) polycrystalline ceramics can be successfully prepared using the classical solid state method. XRD data showed that single $Ca_3Co_4O_9$ phase has been obtained in all samples, while TiC has not been detected due to its low amount. Microstructural observations have confirmed that both phases have not reacted and TiC does not influence sintering process, in agreement with density characterization. On the other hand, electrical resistivity is decreased with TiC addition, reaching the lowest values for the 0.75 wt.% addition, while Seebeck has not been modified in all samples. Thermal conductivity tends to decrease when the temperature is raised in all cases, and the lowest values have been achieved in the 0.25 wt.% TiC samples, which led to an increase of about 40% in ZT values at 800 °C in these samples, when compared with the pure ones. Finally, linear thermal expansion coefficient decreases when TiC content increases. These last data are of the main importance, when considering these materials to build a power generation thermoelectric module, to match the thermal expansion coefficients of all components.

Acknowledgements

The authors wish to thank the Gobierno de Aragón-FEDER (Research Group T 54-17R), and the Spanish MINECO (Ministerio de Economía y Competitividad)-FEDER (Project MAT2017-82183-C3-1-R) for financial support. Authors would like to acknowledge the use of Servicio General de Apoyo a la Investigación-SAI, Universidad de Zaragoza.

REFERENCES

[1] D.M. Rowe, Thermoelectrics Handbook: Macro to Nano, USA, CRC Press, Boca Raton, 2006.
[2] G. Mahan, B. Sales, J. Sharp, Thermoelectric materials: new approaches to an old problem, Phys. Today 50 (1997) 42–47.
[3] H. Naito, Y. Kohsaka, D. Cooke, H. Arashi, Development of a solar receiver for a high-efficiency thermionic/thermoelectric conversion system, Solar Energy 58 (1996) 191–195.

Please cite this article in press as: H. Amaveda, et al., Tuning $Ca_3Co_4O_9$ thermal and transport properties by TiC nanoparticles addition, Bol. Soc. Esp. Cerám. Vidr. (2020), https://doi.org/10.1016/j.bsecv.2020.03.006

[4] M.H. Elsheikh, D.A. Shnawah, M.F.M. Sabri, S.B.M. Said, M.H. Hassan, M.B.A. Bashir, M. Mohamad, A review on thermoelectric renewable energy: principle parameters that affect their performance, Renew. Sustain. Energy Rev. 30 (2014) 337–355.
[5] M. Martín-González, O. Caballero-Calero, P. Díaz-Chao, Nanoengineering thermoelectrics for 21st century: energy harvesting and other trends in the field, Renew. Sustain. Energy Rev. 24 (2013) 288–305.
[6] H. Wang, J. Hwang, M.L. Snedaker, I.-H. Kim, C. Kang, J. Kim, G.D. Stucky, J. Bowers, W. Kim, High thermoelectric performance of a heterogeneous PbTe nanocomposite, Chem. Mater. 27 (2015) 944–949.
[7] C. Zhang, C. Zhang, H. Ng, Q. Xiong, Solution-processed n-type $Bi_2Te_{3-x}Se_x$ nanocomposites with enhanced thermoelectric performance via liquid-phase sintering, Sci. China Mater. 62 (2019) 389–398.
[8] B. Cai, J. Li, H. Sun, L. Zhang, B. Xu, W. Hu, D. Yu, J. He, Z. Zhao, Z. Liu, Y. Tian, Enhanced thermoelectric performance of Na-doped PbTe synthesized under high pressure, Sci. China Mater. 61 (2018) 1218–1224.
[9] X. Wang, H.C. Wang, W.B. Su, F. Mehmood, J.Z. Zhai, T. Wang, T.T. Chen, C.L. Wang, Geometric structural design for lead tellurium thermoelectric power generation application, Renew. Energy 141 (2019) 88–95.
[10] J.Z. Zhai, H.C. Wang, W.B. Su, T. Wang, F. Mehmood, X. Wang, T.T. Chen, T.C. Huo, K.Q. Zhang, C.L. Wang, The p–n transformation and thermoelectric property optimization of $Cu_{1+x}FeSe_2$ ($x = 0$–0.05) alloys, J. Mater. Chem. C 7 (2019) 9641–9647.
[11] H. Kleinke, New bulk materials for thermoelectric power generation: clathrates and complex antimonides, Chem. Mater. 22 (2010) 604–611.
[12] A.C. Sklad, M.W. Gaultois, A.P. Grosvenor, Examination of $CeFe_4Sb_{12}$ upon exposure to air: is this material appropriate for use in terrestrial, high-temperature thermoelectric devices? J. Alloys Compd. 505 (2010) 6–9.
[13] I. Terasaki, Y. Sasago, K. Uchinokura, Large thermoelectric power in $NaCo_2O_4$ single crystals, Phys. Rev. B 56 (1997) 12685–12687.
[14] R. Funahashi, I. Matsubara, H. Ikuta, T. Takeuchi, U. Mizutani, S. Sodeoka, An oxide single crystal with high thermoelectric performance in air, Jpn. J. Appl. Phys. 39 (2000) L1127–L1129.
[15] G. Constantinescu, Sh. Rasekh, M.A. Torres, P. Bosque, M.A. Madre, A. Sotelo, J.C. Diez, Thermoelectric doping effect in $Ca_3Co_{4-x}Ni_xO_9$ ceramics, Bol. Soc. Esp. Ceram. Vidr. 54 (2015) 21–27.
[16] K. Hayashi, K. Sato, T. Nozaki, T. Kajitani, Effect of doping on thermoelectric properties of delafossite-type oxide $CuCrO_2$, Jpn. J. Appl. Phys. 47 (2008) 59–63.
[17] H.C. Wang, C.L. Wang, W.B. Su, J. Liu, Y. Zhao, H. Peng, J.L. Zhang, M.L. Zhao, J.C. Li, N. Yin, L.M. Mei, Enhancement of thermoelectric figure of merit by doping Dy in $La_{0.1}Sr_{0.9}TiO_3$ ceramic, Mater. Res. Bull. 45 (2010) 809–812.
[18] C. Mallada, J.L. Menendez, O.J. Dura, M.A.L. de la Torre, R. Menendez, R. Santamaria, Spark plasma sintered $BaTiO_3$/graphene composites for thermoelectric applications, J. Eur. Ceram. Soc. 37 (2017) 3741–3746.
[19] S. Bresch, B. Mieller, F. Delorme, C. Chen, M. Bektas, R. Moos, T. Rabe, Influence of reaction-sintering and calcination conditions on thermoelectric properties of Sm-doped calcium manganate $CaMnO_3$, J. Ceram. Sci. Technol. 9 (2018) 289–299.
[20] A. Maignan, S. Hebert, M. Hervieu, C. Michel, D. Pelloquin, D. Khomskii, Magnetoresistance and magnetothermopower properties of Bi/Ca/Co/O and Bi(Pb)/Ca/Co/O misfit layer cobaltites, J. Phys. Condens. Matter. 15 (2003) 2711–2723.
[21] H. Itahara, C. Xia, J. Sugiyama, T. Tani, Fabrication of textured thermoelectric layered cobaltites with various rock salt-type layers by using β-$Co(OH)_2$ platelets as reactive templates, J. Mater. Chem. 14 (2004) 61–66.
[22] D. Kenfaui, D. Chateigner, M. Gomina, J.G. Noudem, Anisotropy of the mechanical and thermoelectric properties of hot-pressed single-layer and multilayer thick $Ca_3Co_4O_9$ ceramics, Int. J. Appl. Ceram. Technol. 8 (2011) 214–226.
[23] Y. Liu, Y. Lin, C.-W. Nan, Z. Shen, Preparation of $Ca_3Co_4O_9$ and improvement of its thermoelectric properties by spark plasma sintering, J. Am. Ceram. Soc. 88 (2005) 1337–1340.
[24] A. Sotelo, S.H. Rasekh, G. Constantinescu, M.A. Torres, M.A. Madre, J.C. Diez, Improvement of textured $Bi_{1.6}Pb_{0.4}Sr_2Co_{1.8}O_x$ thermoelectric performances by metallic Ag additions, Ceram. Int. 39 (2013) 1597–1602.
[25] Z. Shi, J. Xu, J. Zhu, Y. Zhang, T. Gao, M. Qin, H. Sun, G. Dong, F. Gao, Effect of platelet template seeds on microstructure and thermoelectric properties of $Ca_3Co_4O_9$ ceramics, Ceram. Int. 45 (2019) 1977–1983.
[26] Z. Shi, F. Gao, J. Xu, J. Zhu, Y. Zhang, T. Gao, M. Qin, M. Reece, H. Yan, Two-step processing of thermoelectric $(Ca_{0.9}Ag_{0.1})_3Co_4O_9$/nano-sized Ag composites with high ZT, J. Eur. Ceram. Soc. 39 (2019) 3088–3093.
[27] G. Cetin, B. Ozcelik, M. Gursul, M.A. Torres, M.A. Madre, A. Sotelo, Effect of annealing and potassium substitution on the thermoelectric and magnetic properties of directionally grown $Bi_2Sr_2Co_2O_y$ ceramics, Bol. Soc. Esp. Ceram. Vidr. (2019), http://dx.doi.org/10.1016/j.bsecv.2019.08.004.
[28] Q. Hu, K. Wang, Y. Zhang, X. Li, H. Song, Enhanced thermoelectric properties of nano SiC dispersed $Bi_2Sr_2Co_2O_y$ ceramics, Mater. Res. Express 5 (2018) 045510.
[29] M. Fan, Y. Zhang, Q. Hu, Y. Zhang, X.-J. Li, H. Song, Enhanced thermoelectric properties of $Bi_2Sr_2Co_2O_y$ by alkali metal element doping and SiC dispersion, Ceram. Int. 45 (2019) 17723–17728.
[30] V. Lankau, H.P. Martin, R. Hempel-Weber, N. Oeschler, A. Michaelis, Preparation and thermoelectric characterization of SiC-B_4C composites, J. Electron. Mater. 39 (2010) 1809–1813.
[31] C. Lorrette, A. Reau, L. Briottet, Mechanical properties of nanostructured silicon carbide consolidated by spark plasma sintering, J. Eur. Ceram. Soc. 33 (2013) 147–156.
[32] G.C. Wei, P.F. Becher, Improvements in mechanical properties in SiC by the addition of TiC particles, J. Am. Ceram. Soc. 67 (1984) 571–574.
[33] D.T. Morelli, Thermal conductivity and thermoelectric power of titanium carbide single crystals, Phys. Rev. B 44 (1991) 5453–5458.
[34] A. Sotelo, F.M. Costa, N.M. Ferreira, A. Kovalevsky, M.C. Ferro, V.S. Amaral, J.S. Amaral, S.H. Rasekh, M.A. Torres, M.A. Madre, J.C. Diez, Tailoring $Ca_3Co_4O_9$ microstructure and performances using a transient liquid phase sintering additive, J. Eur. Ceram. Soc. 36 (2016) 1025–1032.
[35] Y.C. Liou, W.C. Tsai, W.Y. Lin, U.R. Lee, Synthesis of $Ca_3Co_4O_9$ and $CuAlO_2$ ceramics of the thermoelectric application using a reaction-sintering process, J. Aust. Ceram. Soc. 44 (2008) 17–22.
[36] W.M. Haynes, T.J. Bruno, D.R. Lide, CRC Handbook of Chemistry and Physics, CRC Press, Florida, USA, 2016.
[37] E. Woermann, A. Muan, Phase equilibria in the system CaO-cobalt oxide in air, J. Inorg. Nucl. Chem. 32 (1970) 1455–1459.
[38] JCPDS 21-0139.
[39] G.C. Karakaya, B. Ozcelik, M.A. Torres, M.A. Madre, A. Sotelo, Effect of Na-doping on thermoelectric and magnetic performances of textured $Bi_2Sr_2Co_2O_y$ ceramics, J. Eur. Ceram. Soc. 38 (2018) 515–520.

Please cite this article in press as: H. Amaveda, et al., Tuning $Ca_3Co_4O_9$ thermal and transport properties by TiC nanoparticles addition, Bol. Soc. Esp. Cerám. Vidr. (2020), https://doi.org/10.1016/j.bsecv.2020.03.006

[40] Y. Miyazaki, X.Y. Huang, T. Kajitani, Compounds and subsolidus phase relations in the (CaO)–(Co_3O_4)–(CuO) system, J. Solid State Chem. 178 (2005) 2973–2979.
[41] T. Wu, T.A. Tyson, H. Chen, J. Bai, H. Wang, C. Jaye, A structural change in $Ca_3Co_4O_9$ associated with enhanced thermoelectric properties, J. Phys. Condens. Matter 24 (2012) 455602.
[42] D. Sedmidubsky, V. Jakes, O. Jankovsky, J. Leitner, Z. Sofer, J. Hejtmanek, Phase equilibria in Ca–Co–O system, J. Solid State Chem. 194 (2012) 199–205.
[43] L. Boatemaa, J.C. Brouwer, S. van der Zwaag, W.G. Sloof, The effect of the TiC particle size on the preferred oxidation temperature for self-healing of oxide ceramic matrix materials, J. Mater. Sci. 53 (2018) 5973–5986.
[44] N.D. Banu, I. Banu, M.S. Katsiotis, A. Tharalekshmy, S. Stephen, J. Whelan, G.E. Luckachan, R. Vladea, S.M. Alhassan, Identification of selective oxidation of TiC/SiC composite with X-ray diffraction and Raman spectroscopy, Chem. Pap. 70 (2016) 1503–1511.
[45] M.A. Torres, Sh. Rasekh, P. Bosque, G. Constantinescu, M.A. Madre, J.C. Diez, A. Sotelo, Decrease of electrical resistivity in $Ca_3Co_4O_9$ thermoelectric ceramics by Ti doping, J. Mater. Sci. Mater. Electron. 26 (2015) 815–820.
[46] I.V. Matsukevich, A.I. Klyndyuk, E.A. Tugova, et al., Thermoelectric properties of $Ca_{3-x}Bi_xCo_4O_{9+\delta}$ ($0.0 \leq x \leq 1.5$) ceramics, Inorg. Mater. 52 (2016) 593–599.
[47] A.I. Klyndyuk, I.V. Matsukevich, Synthesis, structure, and properties of $Ca_3Co_{3.85}M_{0.15}O_{9+\delta}$ (M = Ti–Zn, Mo, W, Pb, Bi) layered thermoelectrics, Inorg. Mater. 51 (2015) 944–950.
[48] S. Pinitsoontorn, N. Lerssongkram, N. Keawprak, V. Amornkitbamrung, Thermoelectric properties of transition metals-doped $Ca_3Co_{3.8}M_{0.2}O_{9+\delta}$ (M = Co, Cr, Fe, Ni, Cu and Zn), J. Mater. Sci. Mater. Electron. 23 (2012) 1050–1056.
[49] M.A. Torres, G. Garcia, I. Urrutibeascoa, M.A. Madre, J.C. Diez, A. Sotelo, Fast preparation route to high-performances textured Sr-doped $Ca_3Co_4O_9$ thermoelectric materials through precursor powder modification, Sci. China Mater. 62 (2019) 399–406.
[50] M. Sun, K. Wang, N. Sun, X. Zhang, Enhancing the thermoelectric performance of ZnO film by sputter-deposition of Ag nanoparticles, Mater. Res. Express 7 (2020) 015039.
[51] A. Sotelo, Sh. Rasekh, G. Constantinescu, M.A. Torres, M.A. Madre, J.C. Diez, Improvement of textured $Bi_{1.6}Pb_{0.4}Sr_2Co_{1.8}O_x$ thermoelectric performances by metallic Ag additions, Ceram. Int. 39 (2013) 1597–1602.
[52] D. Kenfaui, G. Bonnefont, D. Chateigner, G. Fantozzi, M. Gomina, J.G. Noudem, $Ca_3Co_4O_9$ ceramics consolidated by SPS process: optimisation of mechanical and thermoelectric properties, Mater. Res. Bull. 45 (2010) 1240–1249.
[53] M.A. Madre, F.M. Costa, N.M. Ferreira, A. Sotelo, M.A. Torres, G. Constantinescu, Sh. Rasekh, J.C. Diez, Preparation of high-performance $Ca_3Co_4O_9$ thermoelectric ceramics produced by a new two-step method, J. Eur. Ceram. Soc. 33 (2013) 1747–1754.
[54] H. Wang, X. Sun, X. Yan, D. Huo, X. Li, J.-G. Li, X. Ding, Fabrication and thermoelectric properties of highly textured $Ca_9Co_{12}O_{28}$ ceramic, J. Alloys Compd. 582 (2014) 294–298.
[55] D. Kenfaui, B. Lenoir, D. Chateigner, B. Ouladdiaf, M. Gomina, J.G. Noudem, Development of multilayer textured $Ca_3Co_4O_9$ materials for thermoelectric generators: influence of the anisotropy on the transport properties, J. Eur. Ceram. Soc. 32 (2012) 2405–2414.
[56] M.A. Torres, F.M. Costa, D. Flahaut, K. Touati, Sh. Rasekh, N.M. Ferreira, J. Allouche, M. Depriester, M.A. Madre, A.V. Kovalevsky, J.C. Diez, A. Sotelo, Significant enhancement of the thermoelectric performance in $Ca_3Co_4O_9$ thermoelectric materials through combined strontium substitution and hot pressing process, J. Eur. Ceram. Soc. 39 (2019) 1186–1192.
[57] R. Tian, T. Zhang, D. Chu, R. Donelson, L. Tao, S. Li, Enhancement of high temperature thermoelectric performance in Bi, Fe co-doped layered oxide-based material $Ca_3Co_4O_{9+\delta}$, J. Alloys Compd. 615 (2014) 311–315.
[58] A. Klyndyuk, E. Chizhova, N. Krasutskaya, Thermoelectric ceramics based on the layered cobaltates of bismuth and alkaline-earth metals, Univ. J. Mater. Sci. 5 (2017) 88–94.

Please cite this article in press as: H. Amaveda, et al., Tuning $Ca_3Co_4O_9$ thermal and transport properties by TiC nanoparticles addition, Bol. Soc. Esp. Cerám. Vidr. (2020), https://doi.org/10.1016/j.bsecv.2020.03.006